scientific reports

Check for updates

OPEN

Statistical analysis and forecasting of solar wind parameters across solar cycles

Mu He[1] & Hongbing Zhu[2]✉

This study investigated the statistical properties of solar wind parameters spanning Solar Cycles 20–24, elucidating periodicities that closely aligned with the solar cycle. Significantly, correlations between the smoothed 27-day average value of solar wind parameters and sunspot numbers (SSN) were discerned, shedding light on the intricate interplay between solar activity and solar wind characteristics. Furthermore, the study employed an optimized Long Short-Term Memory (LSTM+) model for forecasting Solar Cycle 25, demonstrating promising predictive capabilities. The analysis predicted the occurrence time of the peak value of SSN in Solar Cycle 25 to be on 27 October 2024 ± 136 days, based on the average relationship with the occurrence time of the trough of Plasma Beta. Notably, observations revealed a double peak in SC-25's solar activity, introducing uncertainty regarding the relative magnitude of each peak.

Keywords Solar cycle, Solar wind, Plasma Beta, LSTM+

The solar wind, a continuous stream of charged particles emitted from the solar corona, plays a crucial role in shaping space weather throughout the solar system. This phenomenon arises from the outward expansion of high-temperature plasma on the solar surface, driven by the complex interplay of the Sun's magnetic fields. Firstly, coronal heating raises the temperature of the corona to several million Kelvin, significantly higher than the solar surface temperature. This extreme heating is achieved through mechanisms such as magnetic reconnection, where magnetic field lines merge and release energy, and wave dissipation, where plasma waves transfer energy to the surrounding particles. These processes ensure that the corona remains sufficiently hot to drive the solar wind[1]. Secondly, in the polar regions of the Sun, magnetic field lines open up, forming structures known as coronal holes. These open magnetic field lines provide pathways for the plasma to escape into space, forming the fast solar wind. The presence of these coronal holes is crucial for the acceleration of the solar wind particles[2]. Thirdly, the high-temperature plasma in the corona undergoes thermal expansion, overcoming the Sun's gravitational pull and escaping into space. This expansion is a fundamental driver of the solar wind, continuously supplying particles that travel throughout the solar system[3]. Moreover, solar activities such as sunspots, solar flares, and coronal mass ejections (CMEs) further modulate the characteristics and intensity of the solar wind. These activities, which are manifestations of the Sun's magnetic field dynamics, can alter the velocity, density, and composition of the solar wind, leading to variations in space weather conditions. For instance, CMEs can significantly enhance the solar wind's density and speed, resulting in geomagnetic storms when they interact with Earth's magnetosphere[4].

The sunspot number (SSN), a measure of the number of sunspots on the solar surface, serves as an indicator of solar activity. SSN varies with the solar cycle, reaching a maximum during the solar maximum and a minimum during the solar minimum. Changes in SSN are closely related to variations in the solar wind and space weather conditions[5]. Various solar wind parameters, such as magnetic field strength, velocity, density, and temperature, have been analyzed to understand their correlation with SSN. Studies have found that the correlation coefficient between the solar wind magnetic field strength and the yearly SSN is quite high, with a value of 0.728, without any time lag. Studies have found that the correlation coefficient between the solar wind magnetic field strength and the yearly SSN is quite high, with a value of 0.728, without any time lag[6]. This indicates a strong direct relationship between these parameters. In contrast, the correlation coefficients for solar wind velocity and temperature with SSN were found to be 0.453 and 0.540, respectively, with time lags of 3 years. This suggests a delayed response of these parameters to the solar activity cycle. The lower correlation between solar wind velocity and SSN might be attributed to the inconsistent response of different velocity levels to solar activity[7]. Furthermore, the solar wind density showed a moderate correlation with SSN, highlighting the varying influence of solar

[1]College of Artificial Intelligence, Suzhou Chien-Shiung Institute of Technology, Suzhou 215411, Jiangsu, China. [2]Avant-Courier Laboratory, Hiroshima 736-0067, Japan. ✉email: chinmumu@gmail.com

cycles on different solar wind parameters. Reconstruction of the magnetopause standoff distance time series for nearly five solar cycles, using both solar wind observations and empirical magnetopause models, revealed that the annual interplanetary magnetic field (IMF) magnitude correlates well with SSN without any time lag. In contrast, the annual solar wind dynamic pressure showed a reasonable correlation with SSN but with a 3-year time lag[8]. Further studies focused on the 11-year solar cycle, represented by the Ca II K index, and its relationship with solar wind dynamic parameters such as speed and dynamic pressure. These studies found a strong anticorrelation between the Ca II K index and both solar wind speed and dynamic pressure during solar cycles 20 and 21. However, this relationship weakened in subsequent cycles 22, 23, and 24[9]. The mean time lag for these correlations was obtained using cross-correlation and mutual information analysis, providing insights into the temporal dynamics of these relationships[10].

Sierra-Porta's research, although focused on Galactic Cosmic Rays, identified SSN positively correlated with both the mean absolute value of the magnetic field strength (|B|) and the Na/Np ratio[11]. The Na/Np ratio, representing the number density of α particles (helium nuclei) relative to the number density of protons (hydrogen nuclei) in the solar wind, is crucial for understanding the relative abundance of helium versus hydrogen within the solar wind. And the Alfvén Mach number (M_A), defined as the ratio of the plasma flow speed to the Alfvén speed (the speed at which Alfvén waves travel through the magnetic field), is particularly relevant in the context of solar wind and CME phenomena, which was found a negative correlation with SSN[12–14]. The Magnetosonic Mach number (M_S), closely linked to the flow velocity of the solar wind, shows periodic variations synchronized with the solar cycle, reflecting the complex interactions of space weather phenomena[15]. A high negative correlation (-0.92) was found between M_S and SSN, as M_S is derived from the interplanetary magnetic field, which tracks SSN closely[16].

Other parameter, such as Plasma Beta, denote the ratio of plasma pressure to magnetic pressure within the solar wind, indicating the predominance of magnetic forces over plasma forces and influencing the behavior of magnetic structures[17]. A low Plasma Beta signified a robust magnetic field with plasma confined within a narrow region, often resulting in a swift, laminar solar wind. Conversely, elevated Plasma Beta levels indicated a weakened magnetic field with more dispersed plasma, potentially leading to a slower, more turbulent solar wind[18]. Furthermore, a significant negative correlation between Plasma Beta and SSN was observed, with plasma beta exhibiting solar cycle variations closely aligned with those of solar wind dynamic pressure, reaching nadirs during periods of peak solar activity. This diminution was particularly pronounced during robust cycle maxima[14]. And Kakad et al.[16] reported a correlation coefficient of − 0.79 for SC-23 and SC-24, while Sierra-Porta[11] identified a significant relationship with an R^2 value of − 0.67 over SC-22 to SC-24.

The interplay between solar activity and solar wind parameters is intricate, yet the periodic fluctuations of solar wind parameters exhibit a close association with the solar cycle. The regularity of the solar cycle can be ascertained and forecasted through an examination of the relationship between solar wind parameters and SSN within the temporal confines of the solar cycle. In this study, we analyzed the temporal relationships between the occurrence of the first peak and maximum value of SSN and the specific timing of solar wind parameters from SC-21 to SC-24, subsequently validating their alignment with documented data for SC-25. We empolyed the optimized LSTM+ model to predict the trend timing of solar wind parameter for SC-25, and subsequently determined the occurrence time of SSN zenith for SC-25.

Solar wind parameters and relationships with SSN

The source of datasets

A periodicity of approximately 27-day aligns with the synodic period of Sun's rotation as observed from Earth (27.3 days), a phenomenon also reflected in various solar indices[19,20]. Consequently, we utilized the average values of every 27 days for solar wind parameters and SSN as our dataset. All Data spanning from 1976 to 2024 were sourced from the official website of NASA's Space Physics Data Facility (SPDF), USA (https://spdf.gsfc.nasa.gov/pub/data/omni/low_res_omni/). Subsequently, the smoothed 27-day average values of all parameters were computed using the following equation[21]. The ensuing data are presented as smoothed 27-day average values, where $\bar{R}(i)$ denotes the *i-th* smoothed 27-day average value.

$$\bar{R}(i) = \frac{1}{12}\left[\frac{1}{2}\left(R_{(i-6)} + R_{(i+6)}\right) + \sum_{j=i-5}^{j=i+5} R(j)\right]$$

The relationships between SSN and solar wind parameters from SC-21 to SC-24

We calculated the Pearson correlation coefficients between each solar wind parameter and SSN across four solar cycles (SC-21 to SC-24). The analysis was conducted for both the entire period and within each individual cycle. Solar wind parameters were then filtered based on correlation coefficients, retaining those with absolute values exceeding 0.6, as shown in Table 1. A significant positive relationship was identified between SSN and both Field Magnitude Average |B| (FMA |B|) and Na/Np. In contrast, SSN exhibited a negative relationship with Plasma Beta, Alfvén Mach number (M_A) and Magnetosonic Mach number (M_S). Detailed descriptions of the solar wind parameters can be found in the document available at this link (https://spdf.gsfc.nasa.gov/pub/data/omni/low_res_omni/omni2.text). Subsequently, Fig. 1 illustrates the periodogram profile obtained from the Rayleigh Power Spectrum algorithm. The analysis revealed notable peaks, particularly around the periods of approximately 10.8 years and 27 days, which are marked in the figure. These peaks indicated significant periodicities within the dataset under examination. This finding is consistent with results obtained using SSN monthly data from SC-22 to SC-24[23], SSN yearly data from 1900–2015[24], and SSN represented by the Wolf number and M_A for the time

		All	SC-21	SC-22	SC-23	SC-24
FMA |B|	Pearson correlation	.788**	.632**	.875**	.857**	.660**
	Sig. (2-tailed)	0.000	0.000	0.000	0.000	0.000
Na/Np	Pearson correlation	.843**	.866**	.908**	.875**	.856**
	Sig. (2-tailed)	0.000	0.000	0.000	0.000	0.000
Plasma Beta	Pearson correlation	−.815**	−.774**	−.928**	−.870**	−.804**
	Sig. (2-tailed)	0.000	0.000	0.000	0.000	0.000
M_A	Pearson correlation	−.895**	−.893**	−.960**	−.911**	−.910**
	Sig. (2-tailed)	0.000	0.000	0.000	0.000	0.000
M_S	Pearson correlation	−.913**	−.963**	−.941**	−.890**	−.907**
	Sig. (2-tailed)	0.000	0.000	0.000	0.000	0.000

Table 1. Results of Pearson Correlation for each solar wind parameter with SSN across all four solar cycles and each solar cycle. **Correlation is significant at the 0.01 level (2-tailed).

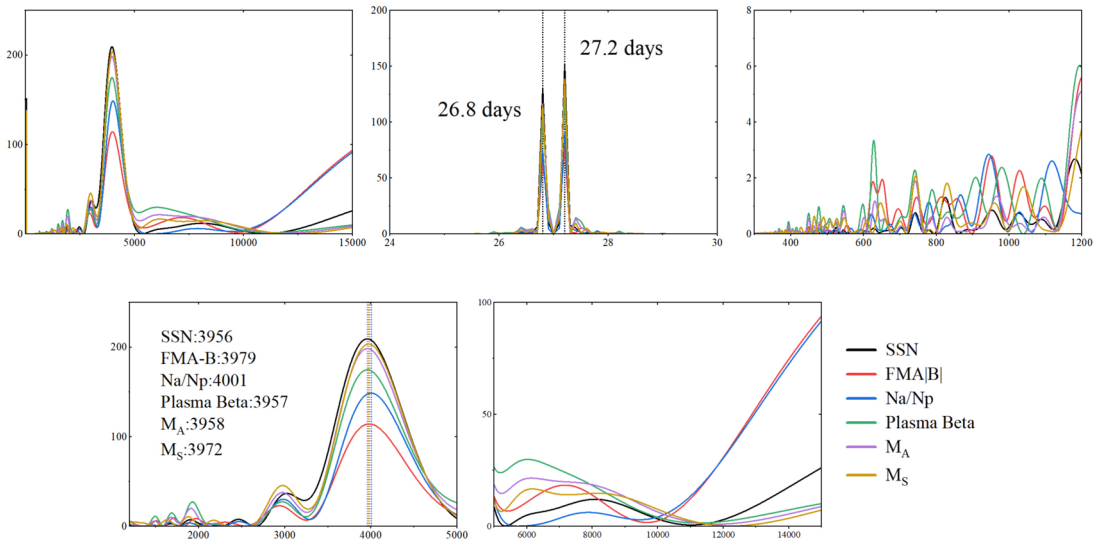

Fig. 1. Periodogram analysis for SSN and solar wind parameters with the Rayleigh Power Spectrum algorithm.

interval 1963 to 2007[12]. Both the correlation and periodicity results indicated that these solar wind parameters exhibit the same stable periodic regularity as SSN.

The relationship between the occurrence period of solar activity increases, as indicated by SSN, and the first peak or trough value of each selected solar wind parameter from SC-21 to SC-24 was investigated and synthesized. A relatively consistent and uniform correspondence was noted where the first peak values of FMA |B| and Na/Np lagged behind the first peak of SSN an average difference of -54 days and 47 days, respectively. Furthermore, the first troughs of M_A, and M_S was observed to occur approximately -33 days and 101 days after the appearance of the first peak of SSN, respectively.

Regression analyses were then conducted with SSN as the dependent variable and each solar wind parameter as the independent variable, as summarized in Table 3. The coefficient results indicated that all solar wind parameters had statistically significant effects on SSN, with p-values below 0.05 across all models. Linear fitting was applied for FMA |B|, Na/Np, and Plasma Beta, resulting in R^2 values of 0.621, 0.711 and 0.665, respectively. Additionally, quadratic fitting formulas were utilized for M_A and M_S, achieving R^2 values of 0.852 and 0.884, respectively.

To validate the relationships derived from Table 2, we compared the actual timing of the first peak for SSN, FMA |B|, and Na/Np, as well as the first trough for M_A and M_S during SC-25. Figure 2 illustrates the comparative results. The calculated time differences and the predicted first peak value of SSN from solar wind parameters based on Table 3 are presented in Table 4. Notably, the peak timings of FMA |B| and Na/Np deviated from the SSN peak by -162 days, while the trough timings of M_A and M_S deviated from the SSN peak by -54 days. These deviations are relatively small compared to the total duration of SC-25 (1259 days), indicating a minor temporal discrepancy. This finding supports the validity of the analyzed relationships between SSN and the timing of these solar wind parameters. This strong agreement between the predicted and actual timing of these solar wind features underscores the robustness of the relationships derived in Table 2 and their potential for space weather prediction.

SC	SSN-P1	|B|-P1	Na/Np-P1	M_A-T1	M_S-T1	SSN-zenith	β-nadir
21	1980-10	1979-132	1980-91	1979-159	1979-186	1980-10	1981-157
22	1989-286	1989-205	1989-205	1989-232	1989-259	1989-286	1991-339
23	2000-76	2000-76	2000-157	2000-103	1999-63	2001-358	2003-303
24	2012-40	2012-148	2012-148	2012-148	2012-229	2014-92	2015-348
Deviation							
21		− 243	81	− 216	− 189		512
22		− 81	− 81	− 54	− 27		783
23		0	81	27	− 378		675
24		108	108	108	189		621
A		− 54	47	− 34	101.25		648

Table 2. The occuring time (year-day) of the first peak (P1) of SSN, FMA |B|(|B|), Na/Np, and the occuring time of the first trough of M_A and M_S, and that of the zenith of SSN and the nadir of Plasma Beta (β). The deviation is the lagged days of solar wind paramter to SSN for each solar cycle (SC) and the average value (A).

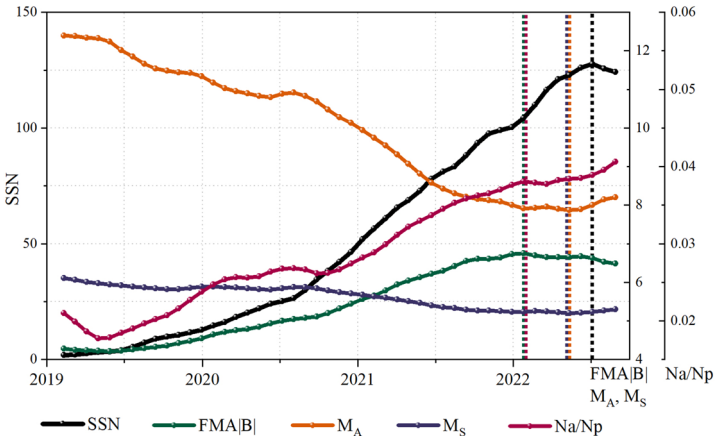

Fig. 2. The comparison of the first peak actual value of SSN with the first peak actual value of FMA |B| and Na/Np, and with the first trough actual value of M_A and M_S in SC-25.

		Unstandardized coefficients		Standardized coefficients			
		B	Std. error	Beta	t	Sig	R Square
FMA |B|(|B|)	|B|	41.786	1.345	0.788	31.063	0.000	0.621
	C	− 180.993	8.784		− 20.605	0.000	
Na/Np	Na/Np	4616.574	121.259	0.843	38.072	0.000	0.711
	C	− 105.196	5.258		− 20.007	0.000	
Plasma Beta (β)	β	− 63.813	1.867	− 0.815	− 34.185	0.000	0.665
	C	240.209	4.786		50.188	0.000	
M_A	M_A	− 185.629	10.540	− 4.551	− 17.612	0.000	0.852
	M^2_A	7.591	0.536	3.662	14.173	0.000	
	C	1148.798	50.524		22.738	0.000	
M_S	M_S	− 1225.705	67.854	− 7.592	− 18.064	0.000	0.884
	M^2_S	95.746	6.022	6.682	15.900	0.000	
	C	3933.640	190.277		20.673	0.000	

Table 3. The regression analyses result with SSN as the dependent variable and each selected solar wind parameter as the independent variable (C is for Constant).

	First peak	First trough	D-days	First peak value (SSN)
SSN	2023/5/6			127.63 (AV)
FMA |B|	2022/11/25		− 162	101.24 ± 3.5 (PV)
Na/Np	2022/11/25		− 162	70.71 ± 3.0 (PV)
M_A		2023/3/13	− 54	158.19 ± 3.2 (PV)
M_S		2023/3/13	− 54	141.88 ± 2.6 (PV)

Table 4. Observed first peak times for SSN, FMA |B| and Na/Np, and first trough times for M_A and M_S in SC-25. Actual value (AV) and predicted value (PV) with ± 95% Confidence Interval are provided for SSN and solar wind parameters at the respective first peak or through. The deviation (D) value represents the lag days of the solar wind parameters relative to SSN.

Additionally, in all four solar cycles analyzed, the nadir of Plasma Beta consistently lagged an average of 557 days behind the zenith of SSN, as detailed in Table 2 and illustrated in Fig. 3. This persistent lag positions Plasma Beta as a viable indicator for predicting the timing of the zenith of SSN in Solar Cycle 25.

Prediction model and results for SC-25 with plasma beta

The prediction model

The LSTM+ model utilized in this study, akin to the conventional LSTM model, was enhanced through parameter fine-tuning, including adjustments to the number of neurons (N), batch size (B), and epochs (E)[25]. A critical optimization step, known as the re-prediction process, was implemented to enhance the forecasting capabilities of the LSTM+ model. In this step, the most recent forecast results from the preceding prediction are used as input data. This approach contrasts with the traditional LSTM method that uses real historical values during training. By using predicted values as inputs, our procedure aims to simulate real-world conditions where future actual values are unavailable. This method helps the model learn to manage its own prediction errors, enhancing its robustness in forecasting future trends. While using actual values during training can confirm the model's performance with historical data, it may not fully demonstrate the model's capacity for predicting unseen trends. Therefore, the forecast represents a projection based on the model's learned patterns, rather than a direct interpolation of historical data. The re-prediction process, where the complete set of forecast outputs from the most recent prediction is used as inputs for the next forecast, enables the LSTM + model to detect subtle variations and improves forecasting accuracy. Through this reforecast procedure, the LSTM + model effectively predicts future trends. Figure 4 illustrates the workflow of the re-prediction procedure, where i denotes the number of forecasts, n is the length of the input, m is the length of the output, x_{t+i} represents the input values, h_{t+i} represents the output values.

The evaluation indicators

An assessment was conducted to determin the relative accuracy of timing and magnitude of solar activity increases in SC-25 and to predict whether the maximum value will higher or lower than that in SC-24, utilizing Plasma Beta as the dataset. Evaluation metrics included the absolute percentage error of the nadir value (ER_V) and the occurring time (ER_D) to quantify prediction accuracy. These evaluation indicators are defined as follows, where V_{AV} represents the nadir value of the actual value, V_{PV} denotes the nadir value of the predicted value, D_{AV} signifies the actual timing of the nadir value occurrence, D_{PV} indicates the predicted timing of the nadir value occurrence.

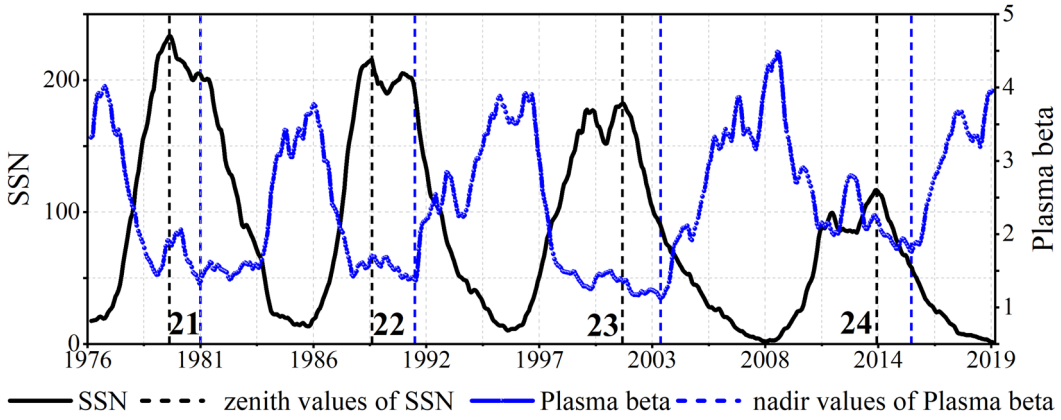

Fig. 3. The relation between SSN and Plasma Beta in the duration from SC-21 to SC-24. The black solid line represents SSN, and the blue line represents Plasma Beta. The vertical dashed black lines are the zenith values of SSN and the vertical dashed blue lines are the nadir values of Plasma Beta in the four solar cycles, respectively.

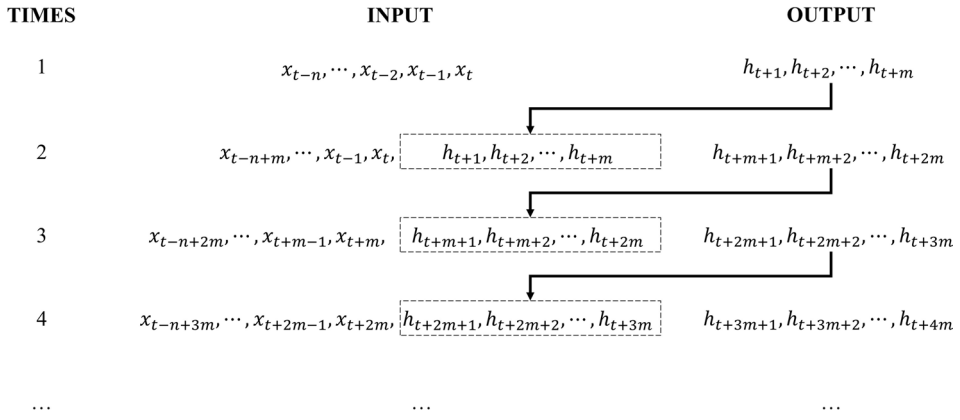

Fig. 4. The workflow of the re-prediction procedure in the LSTM+ model.

$$ER_V = \frac{|(V_{AV} - V_{PV})|}{V_{AV}} \times 100\%$$

$$ER_D = D_{AV} - D_{PV}$$

The predicted results of Plasma Beta in SC-24 and SC-25

Although the solar wind parameter dataset starts from 1963 and includes data from SC-20, there are significant gaps in the data for this cycle. Considering the data completeness and the volume of data required for training the LSTM+ model, we used Plasma Beta data from SC-21 to SC-23 as the training set to predict SC-24. This approach was employed to assess the accuracy of the LSTM+ model predictions. The outcomes of ER_V and ER_D were evaluated across various combinations of input (I) and output (O), N, B, and E setting. In the final assessment, ER_V was determined to be 5.57%, with a 27-day discrepancy (ER_D) between the predicted and actual nadir values for SC-24. Figure 5 illustrates the prediction outcome of the LSTM+ model for SC-24. While the Pearson Correlation coefficient alone does not solely determine predictive capabilities, the higher coefficient (0.793) between predicted (PV) and actual values (AV) obtained from the LSTM+ model for SC-24, underscores a superior predictive dynamic of the LSTM+ model.

The predicted values of Plasma Beta for SC-25 are also illustrated in Fig. 5, juxtaposed with the actual observations during SC-25. The analysis revealed that the predicted occurrence time of the first trough lagged behind the actual date by 91 days. Despite an average error rate of 14.5%, slightly higher than anticipated, the correlation coefficient of 0.98 underscores the accuracy of the predictions. Furthermore, the average correlation coefficient calculated across the entirety of predicted SC-25, compared with SC-21, SC-22, SC-23, and SC-24, stood at 0.88 (with a p-value below 0.05), affirming the robust consistency of the predictive trends with previous cycles. Subsequently, the occurrence time of the zenith value of SSN in SC-25 was estimated based on the average 648-day relationship with the occurrence time of the nadir of Plasma Beta in SC-25 (6 August 2026), resulting in a predicted date of 27 October 2024 ± 136 days according to Table 2. And the first peak of SSN in SC-25 actually

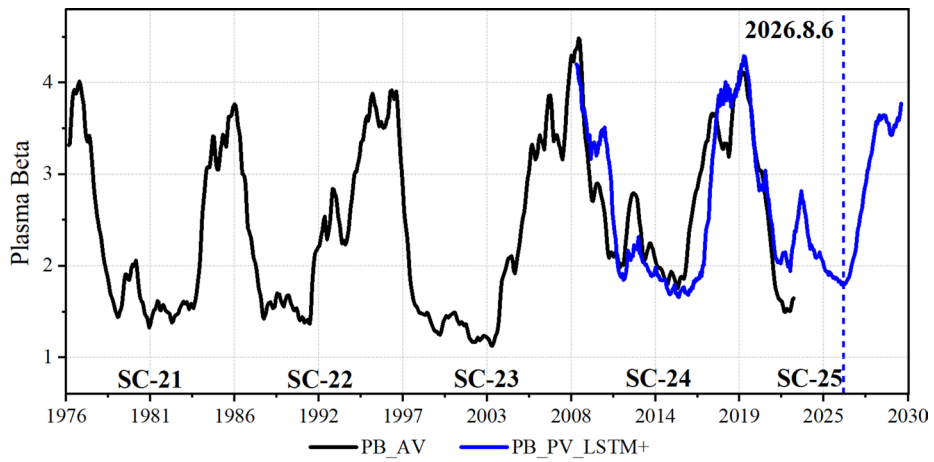

Fig. 5. The prediction result from the LSTM+ model for SC-24 and the prediction result for SC-25.

already occurred on 6 May 2023, deviating by 540 days from the predicted zenith value of SSN, consistent with the average difference between two peaks of preceding four solar cycles (620 days). The predicted trough of Plasma Beta was 1.80, and the predicted peak value of SSN in SC-25 was computed as 125.4 ± 3.9 (95% Confidence Interval), based on the regression results presented in Table 3. The predicted value for the peak sunspot number (SSN) is slightly lower than the revised prediction issued by NOAA's Space Weather Prediction Center (SWPC), which forecasts a peak range of 138 to 166. However, the timing of the predicted peak aligns with the period from May 2024 to February 2025[26].

Conclusion

This study conducted a comprehensive investigation into the intricate relationships between solar wind parameters and solar activity across multiple solar cycles, specifically from SC-21 to SC-25. Utilizing extensive datasets from NASA's Space Physics Data Facility, our analysis provided significant insights into the dynamics of solar variability and its implications for space weather prediction. The findings revealed robust correlations between SSN and various solar wind parameters, all exhibiting an approximate 27-day and 10.8-year periodic regulation. This demonstrated stable periodicities across the four solar cycles under scrutiny. Positive correlations were notably observed for SSN with Field Magnitude Average |B| and Na/Np, while negative correlations were identified with Plasma Beta, M_A and M_S. Regression analyses further elucidated the influence of these solar wind parameters on SSN, emphasizing their statistically significant effects across all models. Linear and quadratic fitting models demonstrated promising predictive capabilities, highlighting the potential for accurate forecasting of solar activity trends based on these parameters.

Of particular significance were the predictions for SC-25, which provided valuable insights into the timing and magnitude of solar activity increases. The analysis forecasted the occurrence time of the zenith of SSN in SC-25 to be on 27 October 2024 ± 136 days, based on the average relationship with the occurrence time of the nadir of Plasma Beta predicted with LSTM + model. This result aligns with the predicted ranges reported in other studies, such as those based on measured fractional areas of the visible solar disk covered by sunspots and plages[27], predictions using the SSN under a bimodal distribution[28], the rush-to-the-poles (RTTP) phenomenon in coronal green line emission as precursors[29], and assimilating poloidal and toroidal magnetic field components derived from synoptic magnetograms into a mean-field dynamo model[30]. Notably, the first observed peak of SSN in SC-25 occurred on 6 May 2023, deviating by 540 days from the predicted zenith date. This deviation is consistent with patterns observed for two previous SSN peaks in the last four cycles. However, it is crucial to acknowledge the inherent uncertainty surrounding this observed peak, as its status as the second-largest or largest peak remains ambiguous based solely on predictive modeling. Further observations and analyses are necessary to conclusively determin the true nature of this peak and its implications for SC-25.

In summary, this study advances our understanding of solar variability and its interaction with solar wind parameters, providing valuable insights for space weather prediction and preparedness. By elucidating the predictive capabilities for SC-25, our findings contribute to improving forecasting accuracy and developing more effective mitigation strategies for potential space weather events. This research underscores the importance of continuing to refine models and observations to better anticipate and manage the impact of solar activity on Earth and space-based technologies.

Data availability

All the data used in our manuscript are from NASA/GSFC's Space Physics Data Facility's OMNIWeb (or CDAWeb or ftp) service, and OMNI data. https://omniweb.gsfc.nasa.gov/.

Received: 4 May 2024; Accepted: 19 August 2024
Published online: 22 August 2024

References

1. Aschwanden, M. J. *Physics of the Solar Corona* (Springer, 2005). https://doi.org/10.1007/3-540-30766-4.
2. Cranmer, S. R. & Winebarger, A. R. The properties of the solar corona and its connection to the solar wind. *Annu. Rev. Astron. Astrophys.* **57**, 157–187 (2019).
3. Parker, E. N. Dynamics of the interplanetary gas and magnetic fields. *Astrophys. J.* **128**, 664 (1958).
4. Hudson, H. *Heliophysics: Space Storms and Radiation: Causes and Effects* (Cambridge University Press, 2010). https://doi.org/10.1017/CBO9781139194532.
5. Hathaway, D. H. The solar cycle. *Living Rev. Sol. Phys.* **12**, 1–87 (2015).
6. Venzmer, M. S. & Bothmer, V. Solar-wind predictions for the Parker Solar Probeorbit: Near-Sun extrapolations derived from an empirical solar-wind model basedon Helios and OMNI observations. *Astron. Astrophys.* **611**, A36 (2018).
7. Li, K. J., Zhanng, J. & Feng, W. A statistical analysis of 50 years of daily solar wind velocity data. *Astron. J.* **151**, 128 (2016).
8. Samsonov, A. A. *et al.* Long-term variations in solar wind parameters, magnetopause location, and geomagnetic activity over the last five solar cycles. *JGR Space Phys.* **124**, 4049–4063 (2019).
9. Reda, R., Giovannelli, L. & Alberti, T. On the time lag between solar wind dynamic parameters and solar activity UV proxies. *Adv. Space Res.* **71**, 2038–2047 (2023).
10. Reda, R. *et al.* The exoplanetary magnetosphere extension in Sun-like stars based on the solar wind–solar UV relation. *Mon. Not. R. Astron. Soc.* **519**, 6088–6097 (2023).
11. Sierra-Porta, D. On the fractal properties of cosmic rays and Sun dynamics cross-correlations. *Astrophys. Space Sci* **367**, 116 (2022).
12. Dmitriev, A. V., Suvorova, A. V. & Veselovsky, I. S. Statistical characteristics of the heliospheric plasma and magnetic field at the Earth's orbit during four solar cycles 20-23. (2013) https://doi.org/10.48550/ARXIV.1301.2929.
13. Luhmann, J. G. *et al.* Solar cycle 21 effects on the interplanetary magnetic field and related parameters at 0.7 and 1.0 AU. *J. Geophys. Res.* **98**, 5559–5572 (1993).
14. Yu, W. *et al.* Small solar wind transients at 1 AU: STEREO observations (2007–2014) and comparison with near-Earth wind results (1995–2014). *J. Geophys. Res. Space Phys.* **121**, 5005–5024 (2016).

15. Freeman, J. W. & Lopez, R. E. Solar Cycle Variations in the Solar Wind. In *Solar Wind-Magnetosphere Coupling 179* (Terra Scientific Publishing Company, 1986).
16. Kakad, B., Kakad, A., Ramesh, D. S. & Lakhina, G. S. Diminishing activity of recent solar cycles (22–24) and their impact on geospace. *J. Space Weather Space Clim.* **9**, A1 (2019).
17. Bourdin, P.-A. Plasma beta stratification in the solar atmosphere: A possible explanation for the penumbra formation. *Astrophys. J. Lett.* **850**, L29 (2017).
18. Cuesta, M. E. *et al.* Compressible turbulence in the near-sun solar wind: Parker solar probe's first eight Perihelia. *Astrophys. J. Lett.* **949**, L19 (2023).
19. Mursula, K. & Zieger, B. The 13.5-day periodicity in the Sun, solar wind, and geomagnetic activity: The last three solar cycles. *J. Geophys. Res.* **101**, 27077–27090 (1996).
20. Mavromichalaki, H., Petropoulos, B., Plainaki, C., Dionatos, O. & Zouganelis, I. Coronal index as a solar activity index applied to space weather. *Adv. Space Res.* **35**, 410–415 (2005).
21. Conway, A. J. Time series, neural networks and the future of the Sun. *New Astron. Rev.* **42**, 343 (1998).
22. Roy, S., Prasad, A., Ghosh, K., Panja, S. C. & Patra, S. N. Chaos and periodicities in solar flare index from Kandilli observatory during 1976–2014. *Res. Astron. Astrophys.* **20**, 110 (2020).
23. Singh, P. R., Tiwari, C. M., Agrawal, S. L. & Pant, T. K. Periodicity variation of solar activity and cosmic rays during solar cycles 22–24. *Sol. Phys.* **294**, 118 (2019).
24. Larocca, P. A. Application of the cross wavelet transform to solar activity and major earthquakes occurred in Chile. *Int J Geosci* **07**, 1310–1317 (2016).
25. Zhu, H., Zhu, W. & He, M. Solar cycle 25 prediction using an optimized long short-term memory mode with F10.7. *Sol. Phys.* **297**, 157 (2022).
26. NOAA's Space Weather Prediction Center (SWPC). *Space weather prediction testbed*. https://testbed.swpc.noaa.gov/products/solar-cycle-progression-updated-prediction-experimental (2024).
27. Penza, V., Berrilli, F., Bertello, L., Cantoresi, M. & Criscuoli, S. Prediction of sunspot and plage coverage for solar cycle 25. *Astrophys. J. Lett.* **922**, L12 (2021).
28. Li, F. Y., Kong, D. F., Xie, J. L., Xiang, N. B. & Xu, J. C. Solar cycle characteristics and their application in the prediction of cycle 25. *J. Atmos. Sol. Terr. Phys.* **181**, 110–115 (2018).
29. Petrovay, K., Nagy, M., Gerják, T. & Juhász, L. Precursors of an upcoming solar cycle at high latitudes from coronal green line data. *J. Atmos. Sol. Terr. Phys.* **176**, 15 (2018).
30. Kitiashvili, I. N. Application of synoptic magnetograms to global solar activity forecast. *Astrophys. J.* **890**, 36 (2020).

Acknowledgements

We acknowledge the use of NASA/GSFC's Space Physics Data Facility's OMNIWeb (or CDAWeb or ftp) service, and OMNI data.

Author contributions

M.H.: research plan, data collection, program code designs, calculations and manuscript writing. H.Z.: initial idea, proposal of critical opinions, integration, revision. All authors participated in the analysis and discussion of the results.

Funding

The authors received no financial support for this article's research, authorship, and publication.

Competing interests

The authors declare no competing interests.

Additional information

Correspondence and requests for materials should be addressed to H.Z.